



Journal of Applied and Computational Mechanics



Research Paper

Experimental Study and Identification of a Dynamic Deformation Model of Dry Clay at Strain Rates up to 2500 s^{-1}

Aleksandr Konstantinov¹, Anatoly Bragov¹, Leonid Igumnov¹,
Victor Eremeyev^{2,3}, Vladimir Vas. Balandin¹, Vladimir Vl. Balandin¹

¹ National Research Lobachevsky State University of Nizhny Novgorod, 23 Gagarin Avenue, building 6, Nizhny Novgorod 603950, Russian Federation

² Department of Mechanics of Materials and Structures, Faculty of Civil and Environmental Engineering, Gdansk University of Technology, 11/12 Gabriela Narutowicza Street, Gdansk, 80-233, Poland

³ Department of Civil and Environmental Engineering and Architecture (DICAAR), University of Cagliari, Via Marengo, 2, 09123 Cagliari, Italy

Received November 28 2021; Revised January 19 2022; Accepted for publication January 19 2022.

Corresponding author: V. Eremeyev (victor.eremeev@pg.edu.pl)

© 2022 Published by Shahid Chamran University of Ahvaz

Abstract. The paper presents the results of an experimental study and numerical simulation of dynamic deformation of dry clay at strain rates of $\sim 10^3 \text{ s}^{-1}$. The main physical and mechanical characteristics of the clay were determined using the modified Split Hopkinson Pressure Bar method for testing of lowly cohesive media in a rigid cage. Three series of experiments were carried out at strain rates of 1400 s^{-1} , 1800 s^{-1} and 2500 s^{-1} . The maximum values of the realized in the experiment axial stresses in clay were about 400 MPa and maximum pressures were 250 MPa. Based on the results of the experiments, the dependences of axial stresses on axial deformations $\sigma_x - \epsilon_x$, shear stresses on pressure $\tau - P$ and pressure on volumetric deformation $P - e$ (curves of volumetric compressibility) were plotted. The shear resistance of clay is noted to be well described by the Mohr-Coulomb law. The obtained deformation diagrams are found to be practically independent of deformation rate. The clay behavior under dynamic loads is shown to be essentially nonlinear. On the basis of the obtained experimental data, a parametric identification of the clay deformation model in the form of Grigoryan's constitutive relation was carried out, which was implemented in the framework of the LS-DYNA software in the form of MAT_SOIL_AND_FOAM model. Using the LS-DYNA computational complex, a numerical simulation of the deformation process of a sample under real experimental conditions was carried out. In the computational experiment, the clay behavior was described by the identified model. Good agreement was obtained between numerical and experimental results.

Keywords: Strain rate, impact loading, measuring bar, dry clay, numerical simulation, experiment, volumetric compressibility, identification.

1. Introduction

Investigation of the impact interaction of deformable and solid bodies with soil media is of great scientific and applied importance. When studying the mechanisms of penetration into soils, both computational and experimental methods are widely used. Computational methods make it possible to simulate and reveal some features of the collision process, which cannot always be detected in the course of experiment. When carrying out calculations, various software systems are employed: LS-Dyna, Ansys, Logos, Abaqus, etc. However, to obtain adequate calculation results, it is necessary to carefully select the existing mathematical models from software systems and set their parameters that most fully reflect the dynamic properties of interacting media. This requires a wide range of experimental studies of the dynamic properties of soil media.

It should be noted that for a number of soil media, the dynamic properties have been studied quite fully. In particular, shock adiabats (axial deformation diagrams) and compressibility curves were obtained for sand in a wide range of load amplitudes [1-11]. Sand shear properties were studied in [12-14]. In these works, for a sandy medium, the effect of moisture, particle size distribution on the shock adiabat parameters, deformation diagrams and yield strengths at high deformation rates $10^2 - 10^5 \text{ s}^{-1}$ and load levels were investigated. The data obtained make it possible to equip mathematical models of sand behavior and precisely set their parameters in a wide range of load changes depending on the initial physical and mechanical characteristics of the sand. A detailed review of experimental studies of the dynamic properties of sand is given in [16]. In [17], the deformation diagrams of clay samples subjected to uniaxial stress were determined experimentally using the Split Hopkinson Pressure Bar (SHPB) method. Clay samples were pre-loaded at different load levels. The experiments were carried out at strain rates ranged from 60 to 600 s^{-1} and stress levels up to 4 MPa. The dynamic strength of the samples and strain fracture are observed to increase with increasing strain rate and preloading value. In [18], wet clay was investigated using the SHPB method within the stress range up to 12 MPa. On the basis of the data obtained, the parameters of the criterion of soil flow in the form of Mohr-Coulomb were determined. In [19], the shock



compressibility of clay with different water content (0%, 4.8%, 7.5%, and 10%) was studied within the pressure range up to 3.5 GPa. According to the results of the experiments, the parameters of shock adiabats were determined, which turned out to be practically the same at different water contents in the samples. In [20], plane-wave experiments were carried out to determine the shock compressibility of loess, the density of which was 1.8 g/cm^3 , and the degree of water saturation was 22%. The shock adiabat was obtained under stress levels ranged from 0.2 to 1.6 GPa. In [21], dynamic studies of plasticine are presented using the SHPB method, which simulates wet clay soil. Deformation diagrams of specimens in a rigid cage in the range of longitudinal stresses up to 150 MPa were obtained. The parameters of the Mohr-Coulomb equation for the plasticine yield point are determined. In [22], the dynamic properties of the wet clay samples in a rigid cage were investigated. The experiments were carried out on a setup with an SHPB in the range of longitudinal stresses up to 200 MPa. Compressibility curves and the dependence of shear stresses on pressure in the Mohr-Coulomb form are obtained. Plane-wave experiments were also carried out to determine the shock adiabat of wet clay in the pressure range up to 2 GPa.

The literature analysis has shown that the dynamic properties of clay soils have not been sufficiently studied. There is a limited number of works devoted to the study of clay properties at high strain rates and high stress amplitudes. This work aims at filling the gap in the region of strain rates $\sim 10^3 \text{ s}^{-1}$.

2. Method of Experimental Research

A modified Split Hopkinson Pressure Bar method is used to carry out dynamic tests of the soil media [12-15]. The scheme of this method is shown in Fig. 1.

The tested soil sample was located between the ends of the measuring bars a rigid cage limiting its radial distribution (Fig. 2). A gas gun, used as a loading device, excites a compression pulse ϵ^I in one of the measuring bars, which, upon reaching the soil sample, loads it. Due to the different acoustic impedances of the bar and the sample, this pulse is split into two pulses - reflected ϵ^R and transmitted through the sample into the second measuring bar ϵ^T . As a result of multiple waves reflection in the sample, its stress-strain state becomes homogeneous, in a time noticeably shorter than the duration of the load.

Since the radial deformation of the sample is impeded by a rigid cage and the radial deformation is much less than the axial one, then, as will be shown below, after some time, an axisymmetric volumetric stress state and a one-dimensional strained state is seen to appear in the sample.

Then the main components of the stress and strain tensors in the sample will have the form:

$$\sigma_1 = \sigma_x; \sigma_2 = \sigma_3 = \sigma_r; \epsilon_1 = \epsilon_x; \epsilon_2 = \epsilon_3 = 0$$

where σ_x and ϵ_x are axial stresses and strains, σ_r is radial stress.

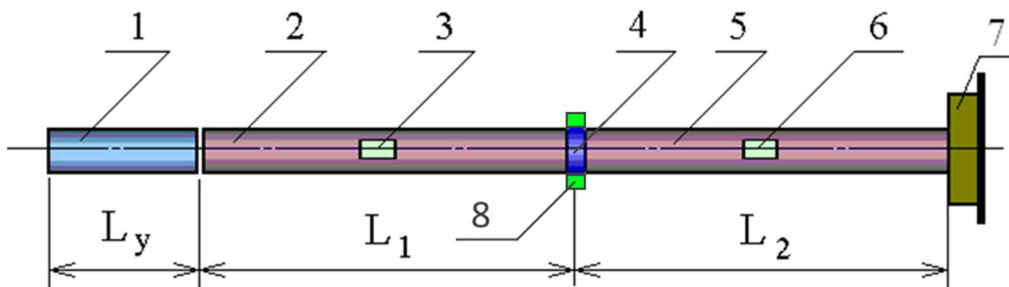


Fig. 1. Scheme of a setup that implements the modified Split Hopkinson Pressure Bar method: 1 - striker, 2 - loading bar, 3 and 6 - strain gauges, 4 - sample, 5 - supporting bar, 7 - damper, 8 - elastic cage

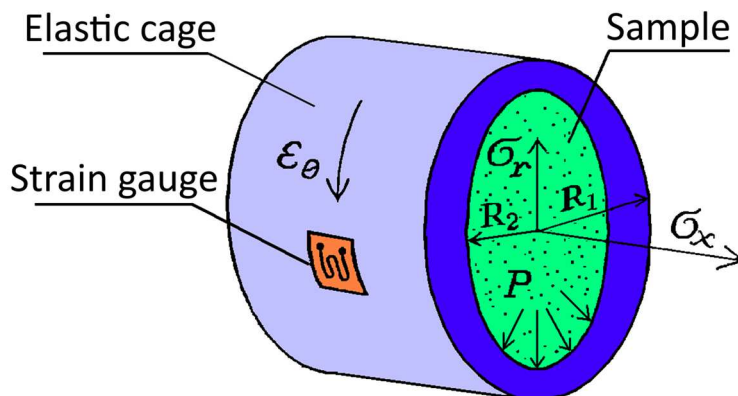


Fig. 2. Cage scheme



The axial components of stress $\sigma_x(t)$, strain $\varepsilon_x(t)$, and strain rate $\dot{\varepsilon}_x(t)$ in the sample are determined by strain gauges that record strain pulses on measuring bars using the traditional SHPB method [23].

$$\sigma_s(t) = \frac{P}{A_s^0} = \frac{EA}{2A_s^0} (\varepsilon^I(t) + \varepsilon^R(t) + \varepsilon^T(t)) \tag{1}$$

$$\dot{\varepsilon}_s(t) = \frac{C}{L_0} \cdot (\varepsilon^I(t) - \varepsilon^R(t) - \varepsilon^T(t)) \tag{2}$$

$$\varepsilon_s(t) = \frac{C}{L_0} \int_0^t (\varepsilon^I(t) - \varepsilon^R(t) - \varepsilon^T(t)) \cdot dt \tag{3}$$

where $\varepsilon^I, \varepsilon^R, \varepsilon^T$ are deformations in incident, reflected and transmitted pulses in measuring bars.

The value of the radial component of the stress tensor can be obtained by solving the problem of elastic deformation of a thick-walled cylinder under the action of internal pressure. The relationship between the internal pressure P_i and the circumferential deformation of the cage $\varepsilon_\theta(t)$ has the form [12]:

$$\sigma_r(t) = P_i(t) = \frac{1}{2R_2^2} [E(R_1^2 - R_2^2) \varepsilon_\theta(t)] \tag{4}$$

where E is Young's modulus of the cage material, R_1 and R_2 are the outer and inner radii of the cage, respectively. The required radial stresses σ_r are the internal pressure P_i , under the action of which the cage undergoes small elastic deformations. Thus, according to the strain gauges readings on the outer surface of the cage $\varepsilon_\theta(t)$, it is possible to determine the radial component of stresses $\sigma_r(t)$ in the sample.

Further, from the obtained parametric dependences $\sigma_x(t)$, $\varepsilon_x(t)$, $\dot{\varepsilon}_x(t)$ and $\sigma_r(t)$, after their mutual synchronization, time as a parameter is excluded and a diagram of uniaxial deformation of the sample $\sigma_x \sim \varepsilon_x$ and the history of the strain rate change $\dot{\varepsilon}_x \sim \varepsilon_x$ are constructed.

The combination of two stress components in the sample, $\sigma_x(t)$ and $\sigma_r(t)$, makes it possible to calculate the basic properties of the tested material.

The maximum shear stresses (shear resistance) will be on planes located at an angle of 45° to the X axis, and their values on these planes will be:

$$\tau(t) = \frac{1}{2} [\sigma_x(t) - \sigma_r(t)] \tag{5}$$

The pressure $P(t)$ in the sample is determined through the principal stresses as follows:

$$P(t) = \frac{1}{3} [\sigma_x(t) + 2\sigma_r(t)] \tag{6}$$

The volumetric deformation will be equal to:

$$\theta(t) = \varepsilon_x(t) \tag{7}$$

Thus, this technique allows one to calculate the following properties of the test material: shear strength $\tau(t)$, lateral pressure (expansion) coefficient $\xi(t)$, pressure $P(t)$ in the sample, volumetric deformation $\theta(t)$, stress intensity $\sigma_i(t)$ and the intensity of deformations $\varepsilon_i(t)$. Therefore, the used version of the SHPB method, in addition to obtaining a diagram of uniaxial compression of a sample under conditions of passive limitation of radial deformation, is used to obtain a curve of volumetric compressibility $P \sim \theta$ and the dependence of shear resistance on pressure $\tau \sim P$.

When loading a soil sample placed in a metal cage, some radial expansion still occurs due to the elastic deformation of the cage; therefore, it is of practical interest to determine the magnitude of radial deformations in order to assess their contribution to volumetric deformation and intensity of deformations.

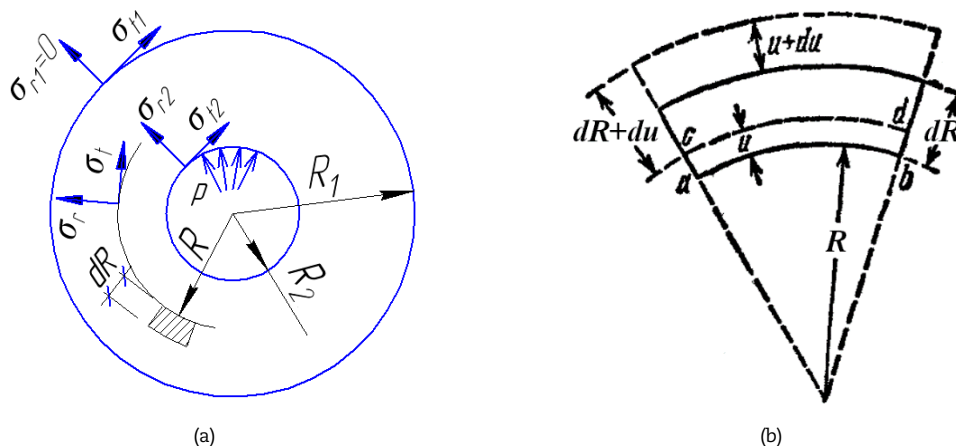


Fig. 3. Determination of the stress-strain state of a thick-walled cylinder



To obtain a theoretical formula that will make it possible to determine the radial deformation of the sample from the deformation impulse recorded on the outer cage surface, let us consider the stress-strain state of a rigid metal cage (Lamé's problem). The cage is a thick-walled elastically deformable cylinder under the action of internal pressure p_i , and the radial stresses of the sample make up the pressure P (Fig. 3 a). The values of tensile stresses and elongation strains will be taken with the plus sign, and, conversely, we will take negative values of the compressive stresses and shortening strains. The values of stresses at points lying on a circle of radius R inside the cylinder wall, which act in the plane of the drawing along the radius σ_r and perpendicular to it σ_t , are determined by the formulas [24]:

$$\sigma_r = \frac{pR_2^2}{R_1^2 - R_2^2} \left[1 - \frac{R_1^2}{R^2} \right]; \quad \sigma_t = \frac{pR_2^2}{R_1^2 - R_2^2} \left[1 + \frac{R_1^2}{R^2} \right]$$

Since the cylinder under consideration does not have a bottom, the third principal stress σ_z , acting in the cage perpendicular to the plane of the drawing (Fig. 3a) and caused by bottom pressure is equal to zero.

The deformation of the cylinder consists in its elongation and in radial displacement of all points of its cross-sections. The elastic deformation of a part of a narrow ring of material with radius R and thickness dR inside the cylinder wall is considered (Fig. 3b). The values of the relative displacements of points lying on a circle of radius R inside the cylinder wall and deformations ε_r and ε_t in the direction of the corresponding stresses σ_r and σ_t [24] will be related by the ratio:

$$\varepsilon_r = \frac{du}{dR} = \frac{1}{E} [\sigma_r - \nu\sigma_t]; \quad \varepsilon_t = \frac{u}{R} = \frac{1}{E} [\sigma_t - \nu\sigma_r]$$

where u is the radial displacement of points lying on a circle of radius R inside the cylinder wall, du is the increase in the thickness of the selected element, and E and ν are the modulus of elasticity and Poisson's ratio of the cage material, respectively.

Thus, the values of stresses σ_{r1} and σ_{t1} at the points of the outer surface of the metal cage and the corresponding relative elongations ε_{r1} and ε_{t1} will be equal (in the notation of physical quantities for points on the outer surface of the cage, we will take index 1):

$$\sigma_{r1} = \frac{pR_2^2}{R_1^2 - R_2^2} \left[1 - \frac{R_1^2}{R_1^2} \right] = 0 \tag{8}$$

$$\sigma_{t1} = \frac{pR_2^2}{R_1^2 - R_2^2} \left[1 + \frac{R_1^2}{R_1^2} \right] = \frac{2pR_2^2}{R_1^2 - R_2^2}$$

$$\varepsilon_{r1} = \frac{1}{E} [\sigma_{r1} - \nu\sigma_{t1}] = -\frac{\nu}{E} \sigma_{t1} \tag{9}$$

$$\varepsilon_{t1} = \frac{1}{E} [\sigma_{t1} - \nu\sigma_{r1}] = \frac{\sigma_{t1}}{E}$$

At points on the inner surface of the metal cage, the values of stresses σ_{r2} and σ_{t2} and the corresponding relative deformations ε_{r2} and ε_{t2} will be equal (in the notation of physical quantities for points on the inner surface of the cage, we take index 2):

$$\sigma_{r2} = \frac{pR_2^2}{R_1^2 - R_2^2} \left[1 - \frac{R_1^2}{R_2^2} \right] \tag{10}$$

$$\sigma_{t2} = \frac{pR_2^2}{R_1^2 - R_2^2} \left[1 + \frac{R_1^2}{R_2^2} \right] \tag{11}$$

$$\varepsilon_{r2} = \frac{1}{E} [\sigma_{r2} - \nu\sigma_{t2}], \quad \varepsilon_{t2} = \frac{1}{E} [\sigma_{t2} - \nu\sigma_{r2}] \tag{12}$$

Since the sample during loading is in close contact with the inner surface of the cage, the value $\varepsilon_{t2} = u_2/R_2$ will be the desired radial deformation of the sample $\varepsilon_{r,specimen}$. The magnitude of the relative elongation ε_{t1} can be determined from the strain gauge readings glued on the outer cage surface ε_0 . To calculate ε_{t2} through the function ε_{t1} , we perform the following mathematical transformations. Substitute expressions (10) and (11) into (12). Then:

$$\varepsilon_{t2} = \frac{1}{E} \left[\frac{pR_2^2}{R_1^2 - R_2^2} \left[1 + \frac{R_1^2}{R_2^2} \right] - \frac{\nu pR_2^2}{R_1^2 - R_2^2} \left[1 - \frac{R_1^2}{R_2^2} \right] \right] = \frac{pR_2^2}{E(R_1^2 - R_2^2)} \left[1 + \frac{R_1^2}{R_2^2} - \nu + \frac{\nu R_1^2}{R_2^2} \right] = \frac{p[R_2^2(1-\nu) + R_1^2(1+\nu)]}{E(R_1^2 - R_2^2)}$$

where

$$p = \frac{E(R_1^2 - R_2^2)}{R_2^2(1-\nu) + R_1^2(1+\nu)} \cdot \varepsilon_{t2} \tag{13}$$

Let us express p in terms of (8), taking into account (9)

$$p = \frac{E(R_1^2 - R_2^2)}{2R_2^2} \cdot \varepsilon_{t1} \tag{14}$$

Equating the right-hand sides of equations (13) and (14), we obtain



$$\frac{E(R_1^2 - R_2^2)}{R_2^2(1 - \nu) + R_1^2(1 + \nu)} \cdot \varepsilon_{t2} = \frac{E(R_1^2 - R_2^2)}{2R_2^2} \cdot \varepsilon_{t1}$$

or finally

$$\varepsilon_{r,specimen}(t) = \frac{R_2^2(1 - \nu) + R_1^2(1 + \nu)}{2R_2^2} \cdot \varepsilon_{\theta}(t) \tag{15}$$

The resulting last formula (19) allows one to determine the radial deformation of the sample $\varepsilon_{r,specimen}$ from the deformation impulse recorded on the outer cage surface ε_{θ} . Taking into account the presence of radial deformation, the values of volumetric deformation and the intensity of sample deformations are determined by the formulas:

$$\theta = \varepsilon_1 + \varepsilon_2 + \varepsilon_3 = \varepsilon_x + 2\varepsilon_r$$

$$\varepsilon_i = \frac{\sqrt{2}}{3} \sqrt{(\varepsilon_1 - \varepsilon_2)^2 + (\varepsilon_2 - \varepsilon_3)^2 + (\varepsilon_3 - \varepsilon_1)^2} = \frac{2}{3} (|\varepsilon_x| + |\varepsilon_r|)$$

To assess the radial deformation, we take the maximum deformation ε_{θ} , measured by strain gauges on the cage surface at the maximum striker speed (30 m/s) equal to 0.001. Using formula (15), we calculate the maximum value of the radial deformation ε_r equal to 0.002. The maximum change in the value of the longitudinal deformation ε_x is 0.2. Thus, the contribution of transverse deformation to volumetric deformation does not exceed 2% of its value and can be neglected. Thus, the assumption of a one-dimensional strained state and bulk stress state is fulfilled.

In the experiments, we used measuring bars with a diameter of 20 mm, made of steel with a yield point of more than 2 GPa. The loading bar was 1500 mm long and the supporting bar 2900 mm long. Small base seam strain gauges were glued on the surface of the loading bar at a distance of 810 mm from the sample, and on the supporting bar at a distance of 420 mm from the sample.

The loading was performed by the impact of a steel bar 300 mm long against the end face of the loading bar. A striker with a diameter of 19.8 mm was accelerated to the required speed in the barrel of a 20 mm gas gun. A pulse shaper made of annealed copper with a thickness of 0.8 mm was placed on the impact end of the measuring bar. This made it possible to obtain sufficiently smooth leading and trailing edges of the incident pulse (Fig. 4).

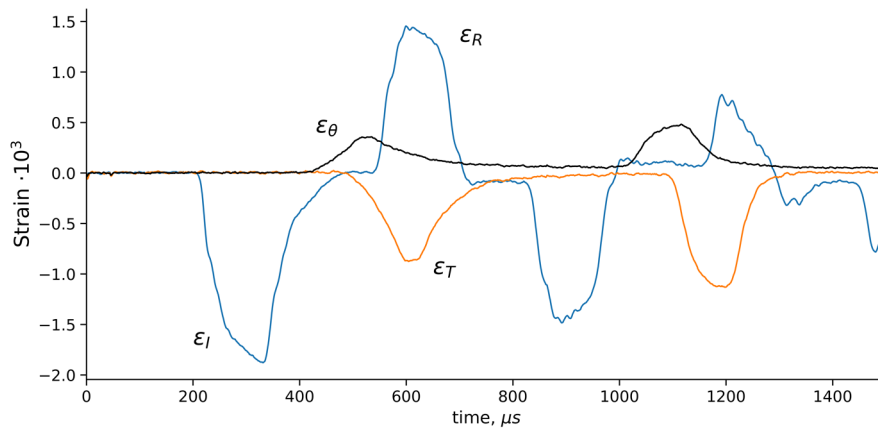


Fig. 4. Strain pulses in measuring bars ($\varepsilon^I, \varepsilon^R, \varepsilon^T$) and cage (ε_{θ}) in experiment No. 51. (ε^I - incident impulse, ε^R - reflected impulse, ε^T - transmitted impulse, ε_{θ} - circumferential deformation impulse in the cage)

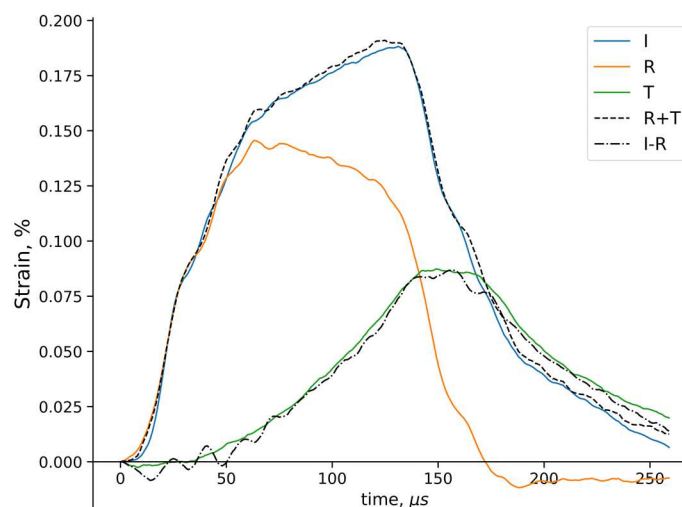


Fig. 5. Synchronized deformation pulses in measuring bars ($\varepsilon^I, \varepsilon^R, \varepsilon^T$) in experiment No. 51



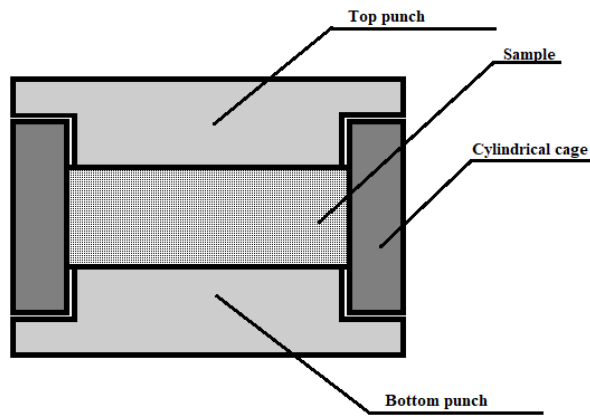


Fig. 6. Diagram of a device for forming a sample

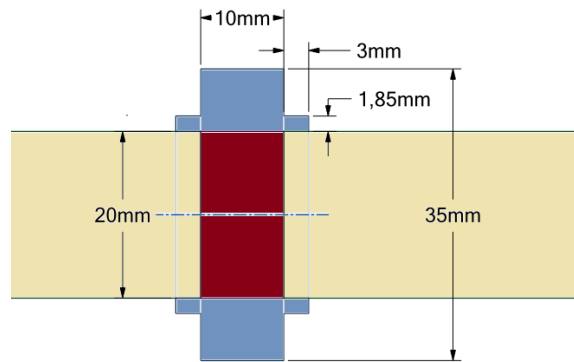


Fig. 7. Measuring cage design

Figure 5 shows synchronized strain impulses in measuring bars. For simplicity all impulses (compressive and tensile) are considered positive. It is clearly seen that the sample is in a state close to homogeneous since the strain values in the transmitted pulse are practically equal to the sum of deformations in the incident and reflected pulses, which indicates the equality of the forces acting on the sample from the side of the loading and supporting bars at each moment of time.

3. Method of Samples Fabrication

The samples were made from clay taken from a depth of 1 m in the Bogorodsky district of Nizhny Novgorod region. The clay was dried in air at room temperature for a long time to completely remove moisture. Then the pieces of clay were crushed to a powdery state. To form the samples, ground clay was mixed with water in an amount of 20% by weight of the clay. The wet clay was thoroughly mixed to ensure uniformity. Clay specimens with a length of about 10 mm were molded in special cylindrical holders (Fig. 6). A strictly defined mass of wet clay was put into a cage between two punches. Then the punches were as close as possible to obtain the required sample volume. After the formation of the sample, the upper punch was removed from the cage. Then the samples were dried in air until the added moisture was completely removed. It should be noted that upon moisture evaporation, the samples shrank in diameter; therefore, the cage diameter for samples forming was selected in such a way that, with complete water evaporation, the samples diameter was 20.5 mm and corresponded to the inner diameter of the cage.

Table 1. The parameters of the tested samples and the experimental conditions

Experiment no.	Sample density g/cm ³	Sample length, mm	Remaining sample length, mm	Striker speed, m/s	Maximum strain rate, s ⁻¹
49	1,95	10,05	8,75	18,9	1470
51	1,96	10,05	8,7	19,4	1360
54	1,97	9,95	8,4	24,9	1710
55	1,98	9,9	8,4	24,9	1830
59	1,97	10,0	8,3	30,6	2630
61	1,98	9,95	8	30,3	2550
65	1,95	9,9	8,4	25,2	1910
66	1,95	9,7	8,1	24,6	1980
67	1,97	9,7	8,65	19,8	1380
68	1,96	9,7	8,4	19,8	1480
69	1,97	9,7	8,6	19,2	1520
70	1,98	9,7	-	30,8	2740
72	1,98	9,7	8,2	24,5	1920
73	1,98	9,7	8,2	24,5	2480
74	1,96	9,8	-	30,3	2480



4. Results of the Experimental Study

After complete drying, the samples were inserted into a cage with strain gauges glued to its external surface for measuring circumferential deformations ϵ_θ . The length of the working part of the cage was 10 mm, so the samples had a length close to that of the working part of the cage. The inner cage diameter was 20.5 mm, which provided a sufficiently small gap between the cage and the side surface of the measuring bars. The outer diameter was 35 mm. Since the lengths of the samples and working part of the cage practically coincided, thin-walled cylinders with a wall thickness of 1.85 mm (Fig. 7) and a length of 5 mm were left at the cage edges to ensure the centering of the cage relative to the bars. As shown in [14], these centering sleeves did not affect the measurement results.

The sample was placed inside the working part of the cage. Then the sample was pressed from both sides with measuring bars to eliminate gaps. The experiments were carried out under three loading modes, differing in the speed of the striker: ~ 20, 25, and 30 m/s. The deformation rate also differed accordingly: 1400, 1800, and 2500 s⁻¹. Five experiments were carried out for each loading mode. The parameters of the tested samples and the experimental conditions are shown in Table 1.

According to the results of experiments using formulas (1-3), the time dependences of longitudinal deformation, longitudinal stress, and strain rate of the sample were determined. By formula (4), the radial stress in the sample was determined as a function of time. These dependencies were used to construct the main diagrams of deformation, the dependence of strain rate on deformation, the dependence of pressure on deformation, as well as the dependence of shear strength on pressure. Pressure P and shear stress τ were determined by formulas (5,6). These dependences for each loading mode were averaged to obtain average curves and standard deviation. Deformation diagrams were obtained in the stress range up to 400 MPa. An example of deformation diagrams and dependences of the strain rate on longitudinal deformation, obtained at a striker speed of close to 20 m/s, is shown in Fig. 8. Technical deformation is plotted along the abscissa.

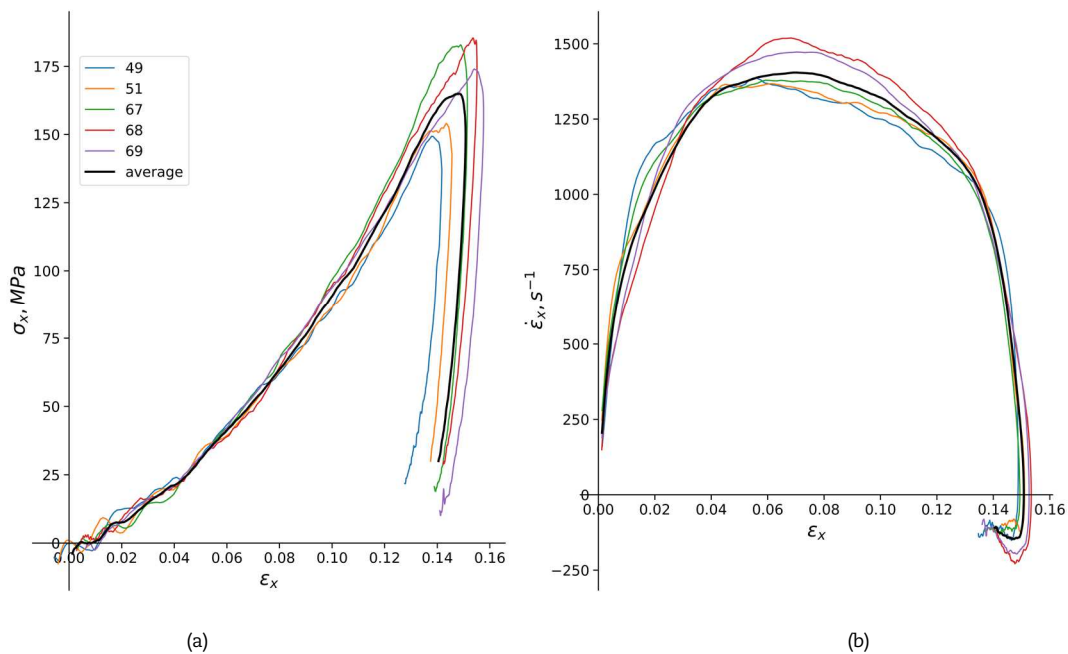


Fig. 8. Deformation diagrams of clay specimens at impact velocities of 20 m/s (a), deformation rate of clay samples at an impact velocities of about 20 m/s (b)

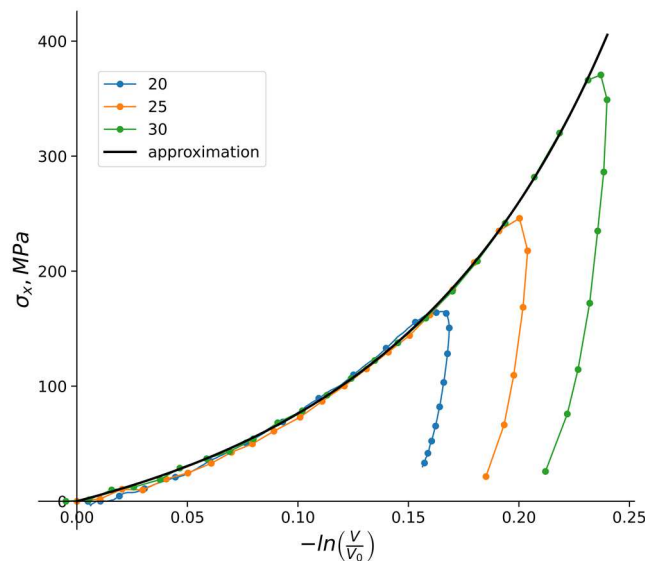


Fig. 9. Deformation diagrams of clay specimens at different impact velocities



Comparison of the obtained average diagrams of clay deformation for different loading conditions is shown in Fig. 9. It is clearly seen that the load branches of the obtained diagrams practically coincide within the scatter of the experimental data, i.e. do not depend on the strain rate, and the values of the achieved stresses and strains depend on the amplitude of the applied load. The slope of the unloading branches of the diagrams is close to linear for different experiments and does not depend on the strain rate.

The loading branch of the true deformation - longitudinal stress dependence can be described by the expression [25]:

$$\sigma_x = \frac{\rho_0 A^2 \epsilon_x}{(1 - B\epsilon_x)^2}$$

where A and B are parameters of the shock adiabat, written in the form $D = A + BU$ (D is the shock wave velocity, B is the mass velocity of the substance behind the front).

The load branches of the diagrams are well approximated by this dependence with the parameters $A = 500$ m/s, $B = 1.9$. The unloading branches of the diagrams have a slope in the linear section, characterized by a modulus of 11300 MPa.

Since the volumetric deformation practically coincides with the longitudinal deformation - the difference is less than 2% of its value, it is possible to construct a summary curve of compressibility in volumetric deformations

The course of the curves characterizing the pressure dependence on volumetric deformation practically does not depend on the strain rate (Fig. 10).

Determination of the shear properties of the studied soil is of considerable interest. For many soil media, the yield point as a function of pressure can be described by the Mohr-Coulomb relation. The dependences τ -P determined in the experiments for the loading mode with an impact velocity of 25 m/s are shown in Fig. 11. It is clearly seen that these dependences have two different branches - loading and unloading, which have different slopes. The averaged dependences of the shear strength τ on the pressure P are shown in Fig. 12.

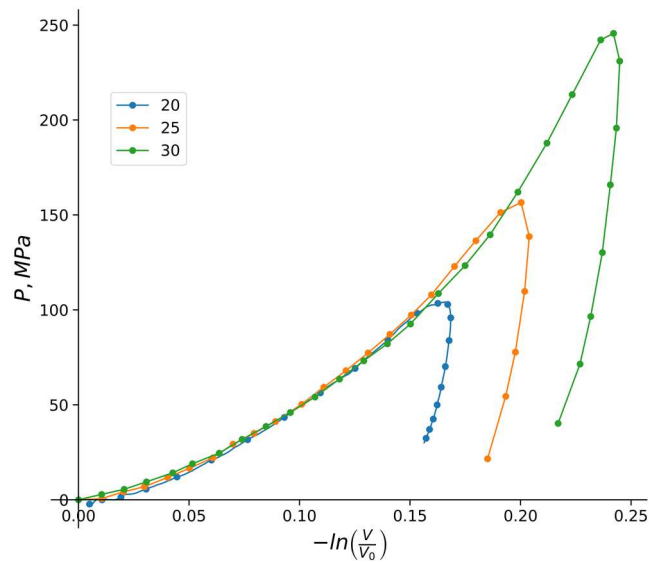


Fig. 10. Pressure versus volumetric deformation at different impact velocities

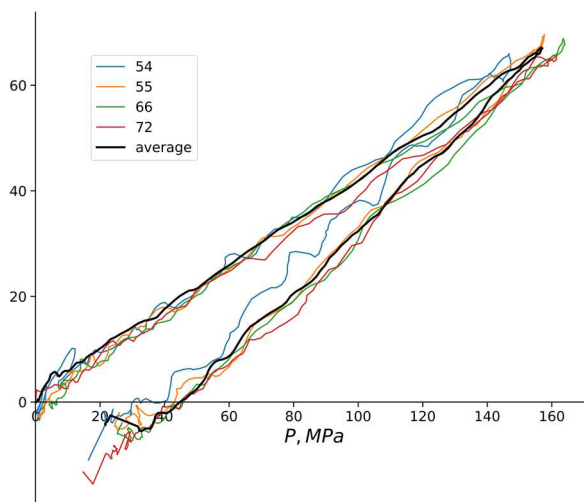


Fig. 11. Shear stress as a function of pressure at impact velocity of 25 m/s



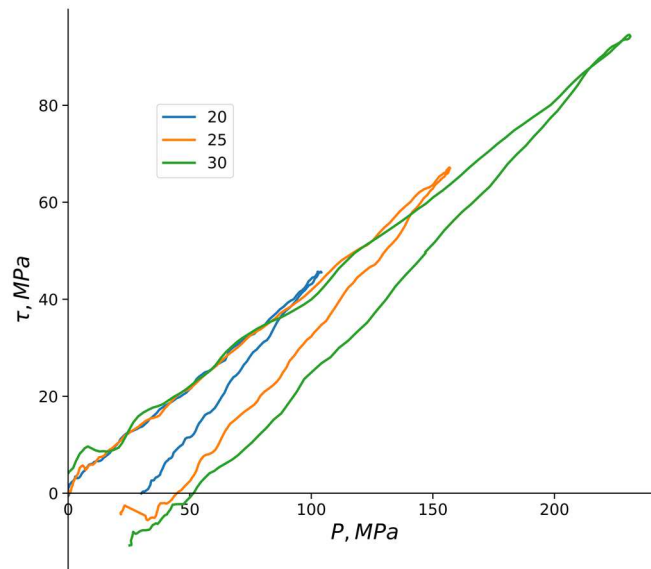


Fig. 12. Shear stress as a function of pressure at different impact velocities

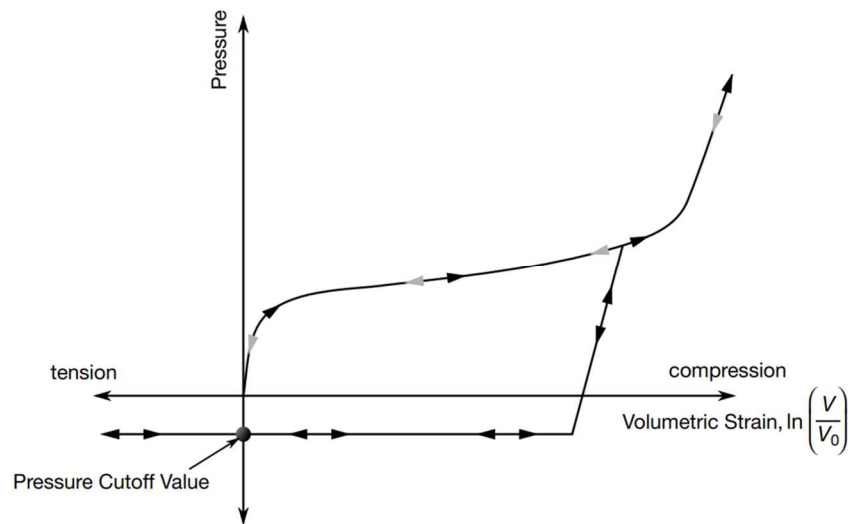


Fig. 13. Curve of volumetric compressibility in the MAT_SOIL_AND_FOAM model [28]

The dependence of the shear strength on pressure in the active load section is described by a linear function of the form $\tau = C + kP$. At projectile velocities of 20 and 25 m/s, $C = 2.5$ MPa, $k = 0.4$, and at an impact velocities of 30 m/s, $C = -0.5$ MPa, and $k = 0.38$. The branches of the τ - P dependence during unloading are well approximated by straight lines with different slopes for different test conditions. At 20 m/s, $C = -19$ MPa, and $k = 0.62$. At 25 m/s, $C = -25$ MPa, and $k = 0.58$. At 30 m/s, $C = -35$ MPa, and $k = 0.53$.

5. Analysis of Experimental Results and Construction of a Mathematical Deformation Model of Clay

A constitutive relation in the form of Grigoryan's model was chosen for modeling the clay behavior [26]. This model is widely used to simulate the behavior of soft soil media under dynamic loads. Soft soil is considered as an elastoplastic medium that provides nonlinear resistance to compression and shear [27]. In this model, to describe the nonlinear behavior of the soil medium, it is necessary to specify the dependence of pressure on volumetric deformation (or density), as well as the dependence of the flow stress on pressure.

In LS-DYNA computational code, a similar model is implemented in the form of material: MAT_SOIL_AND_FOAM [28]. This is a fairly simple model and is recommended for describing soils, concretes, and foams. The volumetric compressibility curve is shown schematically in Fig. 13. As part of the model implementation in LS-DYNA, there are two options for material behavior during unloading. In the first case, unloading occurs along the same curve as the load (gray arrows in Fig. 12). In the second, unloading is performed in a straight line, the slope of which is set by the module of all-round compression K . During tension, the maximum pressure is limited by the *Pressure Cutoff*.

The pressure is considered positive when compressed. Volumetric deformation is determined by the natural logarithm of the relative volume:

$$e = \ln \frac{V}{V_0}$$

here V is the current volume, V_0 is the initial volume. The $P(e)$ curve is specified as a table function.



Table 2. Dependence of pressure on volumetric deformation.

$\ln(V/V_0)$	0	-0.05	-0.1	-0.125	-0.15	-0.175	-0.2	-0.22
P, MPa	0	20	53	75	105	150	220	275

The plastic behavior of the medium is described using the ideal plastic flow function:

$$\phi = J_2 - [a_0 + a_1P + a_2P^2]$$

here J_2 is the second invariant of the stress tensor deviator:

$$J_2 = \frac{1}{2} s_{ij}s_{ij}$$

here s_{ij} are the components of the stress tensor deviator.

On the flow surface:

$$J_2 = \frac{1}{3} \sigma_Y^2$$

where σ_Y is the flow stress at a uniaxial stress state.

Thus:

$$\sigma_Y = [3(a_0 + a_1P + a_2P^2)]^{1/2}$$

The considered model does not imply strain hardening. The plastic behavior of the material is determined by the values of the material parameters a_0, a_1, a_2 .

Model identification for clay was carried out on the basis of data obtained during the experimental determination of the dynamic compressibility of clay using a modified SHPB method described above.

As a result of the performed experimental studies, the dependences of pressure on volumetric deformation, as well as stress intensity on pressure, were obtained for three loading modes, which correspond to striker velocities of 20, 25, and 30 m/s. The dependences of pressure on the logarithm of the relative volume of the sample, grouped by loading modes, are shown in Fig. 10. There is a good repeatability of the results of experiments carried out under the same conditions. Fig. 12 illustrates the shear stress as a function of pressure for three loading modes. It can be noted that the nature of volumetric compressibility curves is practically independent of the loading rate. It should be noted that the unloading curves in the deformation diagrams differ significantly from the load ones. The load branches of the diagrams are actually repeated for different load intensities. The only difference is the maximum volumetric deformation achieved in the test (and, accordingly, the pressure). At the highest strain rate, maximum pressures of the order of 250 MPa appear in the sample. Dependences of stress intensity on pressure in the loading section are practically linear. The slope of these sections is practically independent of the loading rate.

The data shown in Fig. 10 were approximated to equip the MAT_SOIL_AND_FOAM model with the necessary parameters and constants. The left part of Fig. 14 shows the approximation of the curves of volumetric compressibility by a tabular function. The table function itself is presented in Table 2.

Unloading within the framework of the considered model is carried out along a straight line with a given inclination angle. The modulus of the unloading branch was determined by approximating the experimental data (Fig. 14a). The modulus of volumetric compression K during unloading was 11383 MPa.

The procedure for determining the parameters of the Grigoryan's model based on the test data of soft soils in the limiting cage is described in [29].

The loading path parameters on the stress plane under conditions of a uniaxial deformed state can be obtained analytically. The loading path is formed by three segments. The first segment corresponds to the plastic loading of the soil from zero in the initial state to the maximum stress value, determined by the amplitude of the load pulse. The second segment corresponds to the elastic deformation of the soil at the initial stage of unloading from the achieved state. The third segment is associated with the transition of the soil from elastic to plastic state.

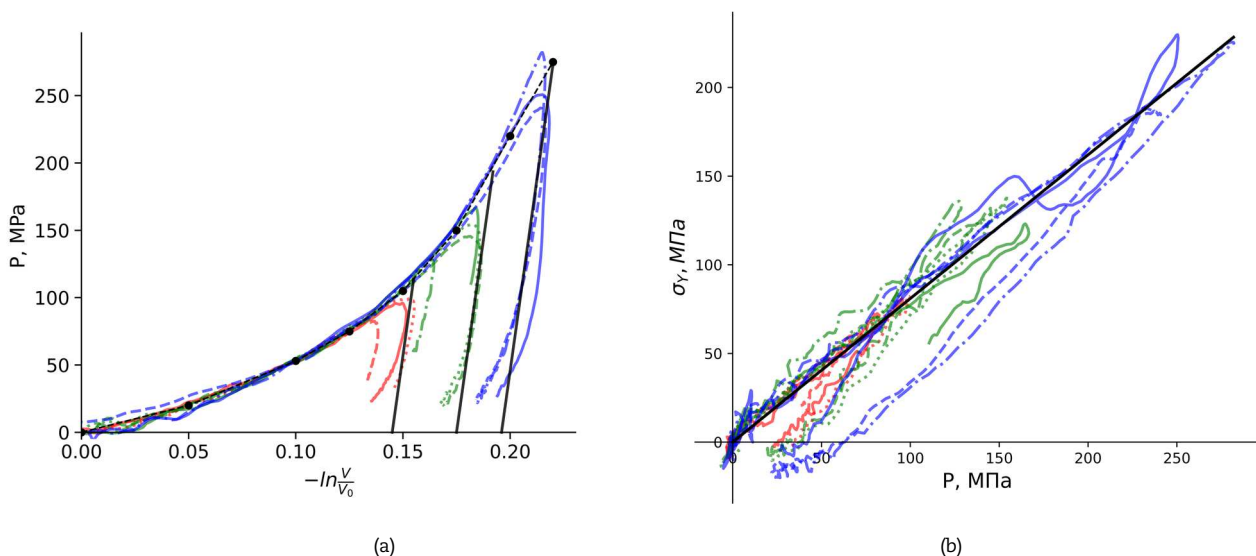


Fig. 14. (a) approximation of the volumetric compressibility curve, (b) - approximation of the dependence of the flow stress on pressure



The slope of the first section is related to the lateral pressure coefficient (determined experimentally), which in turn is related to the coefficient in the linear dependence of the yield stress on pressure. The dependence of the flow stress on pressure is well described by a linear function (Fig. 14b):

$$\sigma_y = k \cdot P + b = 0.81 \cdot P$$

The value of the slope of the first section of the loading path:

$$K_I^\sigma = \frac{d\sigma_r}{d\sigma_x} = \frac{1 - \frac{k}{3}}{1 + 2 \cdot \frac{k}{3}}$$

For $k = 0.81$, we get $K_I^\sigma = 0.474$.

The slope of the second section (elastic) is determined by the formula, which for $G = \beta \cdot k \cdot K/2$, where K & G – volumetric and shear unloading modules will have the form:

$$K_{II}^\sigma = \frac{K - 2G/3}{K + 4G/3} = \frac{1 - k \cdot \beta/3}{1 + 2 \cdot k \cdot \beta/3}$$

where β is a numerical parameter determined experimentally.

In the case of the tested soil, the value $\beta = 1.32$ gives a good approximation of the experimental data on the elastic section of the unloading branch (Fig. 6). Thus, $G = 6085$ MPa, $K_{II}^\sigma = 0.376$.

The third (plastic) section of the loading path has a slope:

$$K_{III}^\sigma = \frac{1 + k/3}{1 - 2 \cdot k/3}$$

For $k = 0.81$, we get $K_{III}^\sigma = 2.76$.

The thus constructed approximation of the experimental loading trajectory by the three-link model is shown in Fig. 15.

It should be noted that the indicated solution was obtained analytically for the case of one-dimensional deformation of the sample. Since the cage in real experiments is pliable and undergoes elastic deformations, the parameter β was determined by selection when modeling the deformation process of the sample in the confining cage. The value of the parameter obtained using the analytical solution was taken as the initial approximation. The simulation scheme is described in detail below. Figure 16 illustrates the deformation trajectory of the sample in the $\sigma_x - \sigma_r$ axes for different values of the β parameter. It can be seen that the best agreement with the experimental data is observed at $\beta = 1.13$, which corresponds to the unloading shear modulus $G = 5200$ MPa.

The coefficients of the MAT_SOIL_AND_FOAM model are determined as follows:

$$a_0 = \frac{\sigma_0^2}{3} = 75, a_1 = \frac{2 \cdot k \cdot \sigma_0^2}{3} = 8.26, a_2 = \frac{k^2}{3} = 0.2187$$

here σ_0 is the dynamic yield stress of clay, determined by using the classical version of the SHPB method in compression under conditions of a uniaxial stress state. The average value of this stress in the dynamic range of strain rates was about 15 MPa.

The complete set of model constants, presented in the form of an input map of the LS DYNA PP, is shown in Fig. 17.

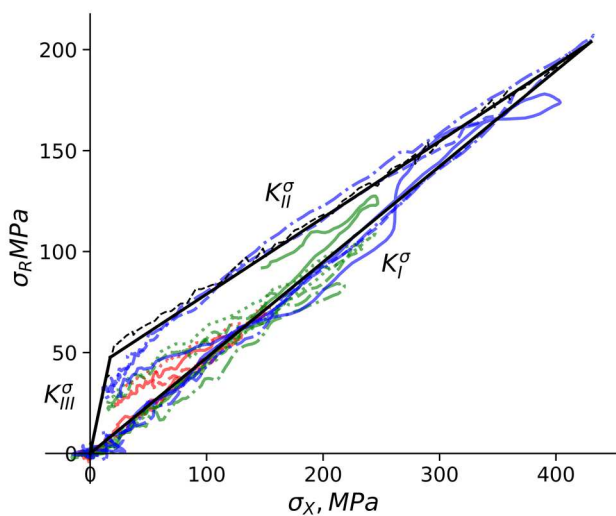


Fig. 15. Approximation of the clay loading trajectory

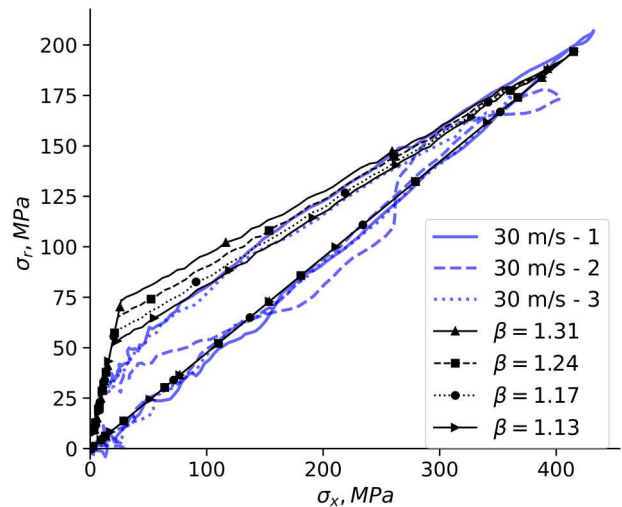


Fig. 16. Determination of the parameter β taking into account the cage flexibility



Table 3. Model parameters for describing the behavior of measuring bars and a cage.

	Density, kg/m ³	Young's modulus, MPa	Poisson's ratio
Measuring bars	8050	185000	0.28
Cage	7850	210000	0.28

6. Results of Numerical Simulation of Sample Compression in the Cage

Experiments on shock compression of clay specimens in a confining cage were numerically reproduced using the LS-DYNA PP. Figure 18 shows a fragment of the model: the area near the sample in the bounding cage. The numbers indicate: 1 - cage, 2 - measuring bars, 3 - sample. Geometric dimensions are given on Fig. 7. The length of the loading measuring bar in the computational experiment, as in the full-scale test, was 1.5 m, and that of the reference bar, 2.9 m. In the experiments, measuring bars with a diameter of 20 mm made of high-strength steel were used. Since the measuring bars and the cage within the framework of the method work in the elastic region, their behavior was described by the linear elastic MAT_ELASTIC models. Model parameters are shown in Table 3.

The behavior of a clay sample, as mentioned above, was described by the MAT_SOIL_AND_FOAM model, the parameters of which were defined earlier. Since the behavior of the material did not show a visible dependence on the strain rate, an experiment was simulated with the maximum load amplitude (striker speed - 30 m/s). A pressure pulse $\sigma_L(t)$ acting on the end face of the loading bar was set as the load. The shape of this impulse was determined from the incident deformation impulse recorded in the corresponding full-scale test according to the formula:

$$\sigma_L(t) = -E \cdot \epsilon^I(t)$$

here E is the modulus of elasticity of the measuring bar, $\epsilon^I(t)$ is the deformation impulse recorded in the measuring bar.

The resulting time dependence of the voltage pulse is shown in Fig. 19.

The problem was solved in an axisymmetric setting. An explicit scheme was used to integrate the equations over time. Area-weighted axisymmetric Lagrangian finite elements (type 14) were used to discretize the space.

Figure 20 (a-d) provides a comparison of simulation results and field test data. The components of the stress tensor in the computational cell corresponding to the sample were determined numerically. Blue lines in the figures correspond to field test data, black lines correspond to simulation results. In Fig. 20a pressure versus strain is compared. Figure 20b shows curves in axial stress-radial stress axes. Figures 20c and 20d compare the time dependences of axial and radial stresses in the sample, respectively. In general, it can be noted that the identified mathematical model based on the results of the experiment allows quite accurately, both qualitatively and quantitatively, to reproduce the main features (including nonlinear behavior) of the material under study.

```

*MAT_SOIL_AND_FOAM_TITLE
glay
$#      mid      ro      g      bulk      a0      a1      a2      pc
        3      0.00198      5200      11383      75      8.26      0.227
$#      vcr      ref      lcid
        0.0      0.0      0
$#      eps1      eps2      eps3      eps4      eps5      eps6      eps7      eps8
        0.00e+00      -5.00e-02      -1.00e-01      -1.25e-01      -1.50e-01      -1.75e-01      -2.00e-01      -2.20e-01
$#      eps9      eps10
        0.0      0.0
$#      p1      p2      p3      p4      p5      p6      p7      p8
        0.000e+00      2.000e+01      5.300e+01      7.500e+01      1.050e+02      1.500e+02      2.200e+02      2.750e+02
$#      p9      p10
        0.0      0.0
    
```

Fig. 17. Parameters of the clay model for PP LS-DYNA

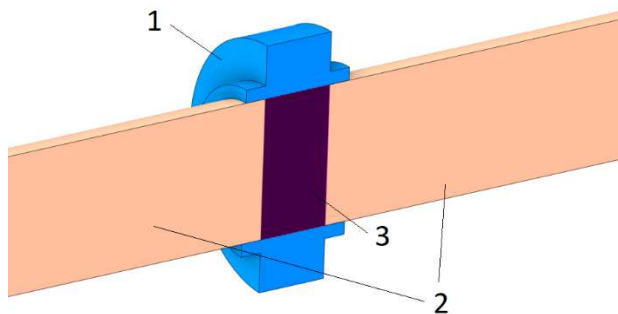


Fig. 18. Fragment of the model

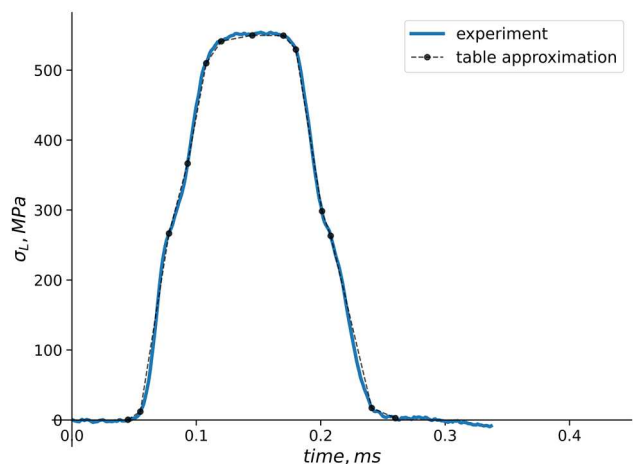


Fig. 19. Voltage impulse (load)



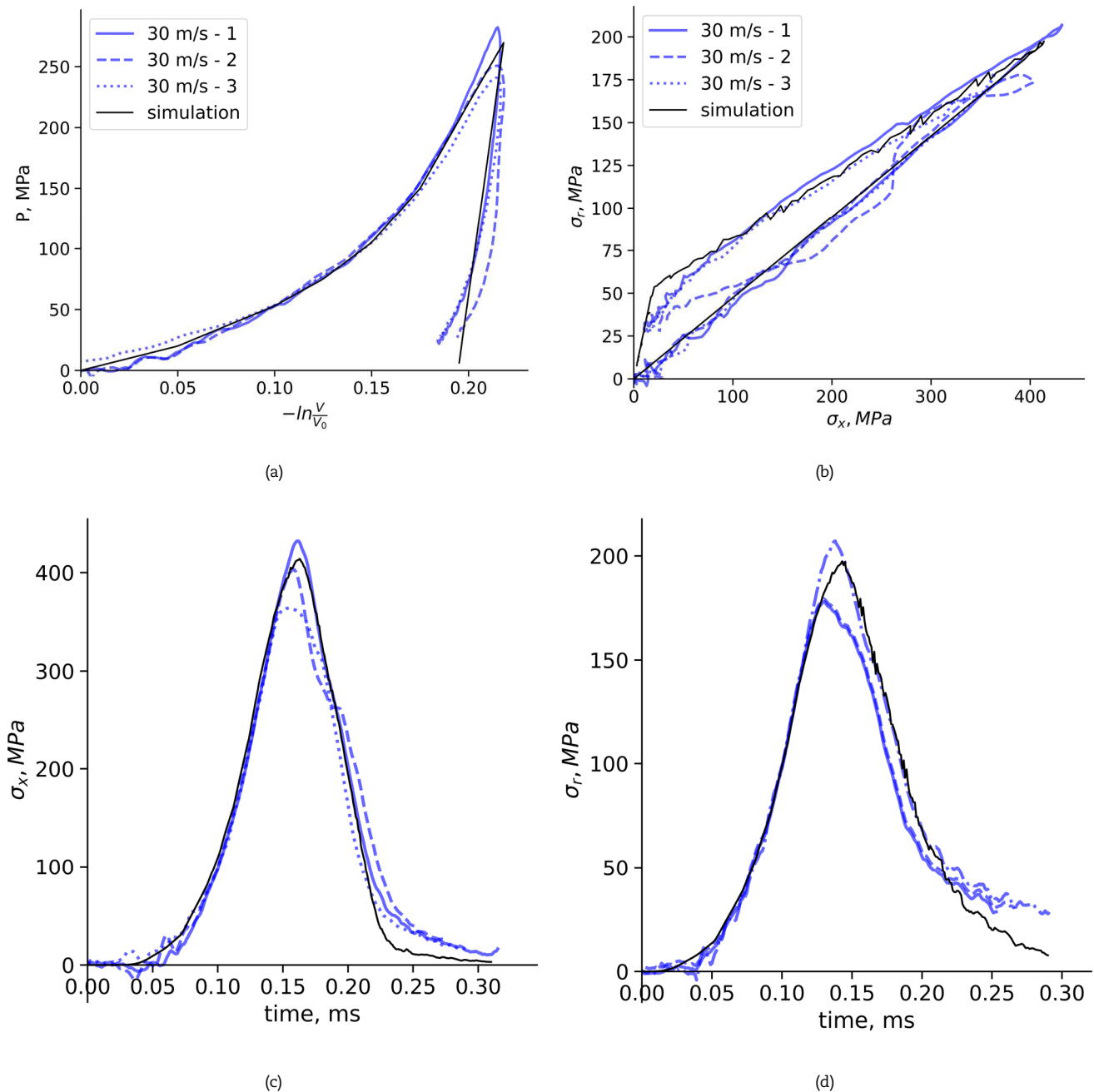


Fig. 20. Comparison of simulation results and field tests

7. Conclusion

It was found in the experiments that the deformation diagrams and compressibility curves of the studied soil practically coincide in the load section at different strain rates in the range of 1300-2500 s⁻¹. It should be noted that similar behavior is typical for other types of soils (in particular, for sandy ones). The unloading branches of the deformation diagrams and compressibility curves under different loading conditions also have a similar slope, which does not depend on the strain rate. The dependence of the shear strength on pressure for dry clay is also practically independent of the strain rate. Comparison with the results for wet clay [22] shows that wet clay has a much lower compressibility than dry clay, while when wet clay is compressed, maximum stresses are achieved at deformations that are significantly lower than for dry clay. The shear strength for wet clay is also significantly lower than for dry clay. The coefficient K , which determines the slope in the Mohr-Coulomb law, is two times higher (0.4) for dry clay than for wet clay (0.2). The experimental information obtained was used to identify the parameters of the material model in the Grigoryan form. Numerical simulation of dynamic tests has shown that the identified model makes it possible to adequately describe the behavior of clay under dynamic load when the sample is in a confined state. Further refinement of the model is planned to be carried out using experiments under uniaxial stress conditions.

Author Contributions

V. V. Balandin and V.I. Balandin conducted experiments and analyzed the results. A. Konstantinov engaged in the model identification and numerical simulation. A. Bragov proposed a modified experimental scheme. L. Igumnov carried out the general management of the study. V. Eremeyev engaged in the interpretation of experimental data and the results of numerical simulation.



All authors made a substantial, direct and intellectual contribution to this work. The manuscript was written through the contribution of all authors. All authors discussed the results, reviewed and approved the final version of the manuscript.

Acknowledgments

Not Applicable

Conflict of Interest

The authors declared no potential conflicts of interest concerning the research, authorship, and publication of this article.

Funding

The reported experimental study and model identification was funded by RFBR, project number 20-38-70091. The numerical simulation was done with support by RSF, project number 21-19-00283.

Data Availability Statements

The datasets generated and/or analyzed during the current study are available from the corresponding author on reasonable request.

References

- [1] Lagunov, V.A., Stepanov, V.A. Measurements of the dynamic compressibility of sand under high pressures, *Zh. Prikl. Mekh. Tekhn. Fiz. (J. Appl. Mech. Tech. Phys.)*, 1, 1963, 88-96 (Engl. Transl.).
- [2] Bragov, A.M., Balandin, V.V., Lomunov, A.K., Filippov, A.R. Determining the impact compressibility of soft soils from reversed test results, *Tech. Phys. Lett.*, 32(6), 2006, 487-86. <https://doi.org/10.1134/S1063785006060101>.
- [3] Bragov, A.M., Grushevskii, G.M. Influence of the moisture content and granulometric composition on the shock compressibility of sand, *Tech. Phys. Lett.*, 19, 1993, 385-6.
- [4] Arlery, M., Gardou, M., Fleureau, J.M., Mariotti, C. Dynamic behaviour of dry and watersaturated sand under planar shock conditions, *Int. J. Impact Eng.*, 37, 2010, 1-10. <https://doi.org/10.1016/j.ijimpeng.2009.07.009>.
- [5] Bragov, A.M., Lomunov, A.K., Sergeichev, I.V., Tsembelis, K., Proud, W.G. Determination of physicommechanical properties of soft soils from medium to high strain rates, *Int. J. Impact Eng.*, 35(9), 2008, 967-76.
- [6] Song, B., Chen, W., Luk, V. Impact compressive response of dry sand, *Mech. Mater.*, 41, 2009, 777-85. <https://doi.org/10.1016/j.mechmat.2009.01.003>.
- [7] Martin, B.E., Chen, W., Song, B., Akers, S.A. Moisture effects on the high strain-rate behavior of sand, *Mech. Mater.*, 41, 2009, 786-98. <https://doi.org/10.1016/j.mechmat.2009.01.014>.
- [8] Martin, B.E., Kabir, M.E., Chen, W. Undrained high-pressure and high strain-rate response of dry sand under triaxial loading, *Int. J. Impact Eng.*, 54, 2013, 51-63. <https://doi.org/10.1016/j.ijimpeng.2012.10.008>.
- [9] Chapman, D.J., Tsembelis, K., Proud, W.G. The behavior of water saturated sand under shock-loading, *Proceedings of the 2006 SEM annual conference and exposition on experimental and applied mechanics*, 2, 2006, 834-40.
- [10] Luo, H., Cooper, W.L., Lu, H. Effects of particle size and moisture on the compressive behavior of dense Eglin sand under confinement at high strain rates, *Int. J. Impact Eng.*, 65, 2014, 40-55. <https://doi.org/10.1016/j.ijimpeng.2013.11.001>.
- [11] Dianov, M.D., Zlatin, N.A., Mochalov, S.M., et al. Shock compressibility of dry and watersaturated sand, *Sov. Tech. Phys. Lett.*, 2, 1977, 207-8.
- [12] Bragov, A.M., Grushevsky, G.M., Lomunov, A.K. Use of the Kolsky method for studying shear resistance of soils, *DYMAT J.*, 1(3), 1994, 253-259.
- [13] Bragov, A.M., Grushevsky, G.M., Lomunov, A.K. Use of the Kolsky Method for Confined Tests of Soft Soils, *Exp. Mech.*, 36, 1996, 237-242.
- [14] Bragov, A.M., Kotov, V.L., Lomunov, A.K., Sergeichev, I.V. Measurement of the dynamic characteristics of soft soils using the Kolsky method, *J. Appl. Mech. Tech. Phys.*, 45(4), 2004, 580-5. <https://doi.org/10.1023/B:JAMT.0000030338.66701.e9>.
- [15] Bragov, A.M., Iuzhina, T.N., Lomunov, A.K., Igumnov, L., Belov, A., Eremyev, V.A. Investigation of Wood Properties at Elevated Temperature, *J. Appl. Comput. Mech.*, 8(1), 2022, 298-305.
- [16] Omidvar, M., Iskander, M., Bless, S. Stress-strain behavior of sand at high strain rates, *Int. J. Impact Eng.*, 49, 2012, 192-213. <https://doi.org/10.1016/j.ijimpeng.2012.03.004>.
- [17] Yang, R., Chen, J., Yang, L., Fang, S., Liu, J. An experimental study of high strain-rate properties of clay under high consolidation stress, *Soil Dyn. Earth. Eng.*, 92, 2017, 46-51.
- [18] He, Y.X., Luan, G.B., Zhu, Zh.W. Dynamic Constitutive Modeling of Partially Saturated Clay under Impact Loading, *Int. J. Nonlin. Sci. Num. Simul.*, 11, 2010, 195-199.
- [19] Gang, Z., Li, Y., Jin, L., Wu, Z., Wu K., Jing, J., Tan, S., Qian, B., Zhu, Y., Zhang, X. Dynamic behavior of clay with different water content under planar shock conditions, *Int. J. Impact Eng.*, 129, 2019, 57-65. <https://doi.org/10.1016/j.ijimpeng.2019.03.001>.
- [20] Li, Y., Zhu, Y., Zhang, X., Li, J., Wu, K., Jing, J., Tan, S., Zhou, G. Dynamic behavior of remolded loess under planar shock conditions, *Int. J. Impact Eng.*, 111, 2018, 236-243. <https://doi.org/10.1016/j.ijimpeng.2017.09.016>.
- [21] Bragov, A.M., Gandurin, V.P., Grushevskii, G.M., Lomunov, A.K. New Potentials of Kol'skii's Method for Studying the Dynamic Properties of Soft Soils, *J. Appl. Mech. Tech. Phys.*, 36(3), 1996, 476-481. <https://doi.org/10.1007/BF02369791>.
- [22] Bragov, A.M., Demenko, P.V., Kruszka, L., Lomunov, A.K., Sergeichev, I.V. Évaluation de la compressibilité dynamique et de la résistance au cisaillement pour une large gamme de pressions et de vitesses de déformation Investigation of dynamic compressibility and shear resistance of soft soils in a wide range of strain rate and pressure, *Fifth European Conference "Numerical Methods in Geotechnical Engineering" NUMGE*, Mestast (ed.), Presses de l'ENPC/LCPC, Paris, 2002.
- [23] Kolsky, H. An investigation of the mechanical properties of materials at very high rates of loading, *Proc. Phys. Soc., Lond. B*, 62, 1949, 676-700.
- [24] Belyaev, N.M. *Strength of materials*, Moscow, Nauka, 1976.
- [25] Zeldovich, Ya.B., Raizer, Yu.P. *Physics of shock waves and high-temperature hydrodynamic phenomena*, Courier Corporation, 2002.
- [26] Grigoryan, S.S. Ob osnovnykh predstavleniyakh dinamiki gruntov [Basic concepts of soil dynamics], *Prikladnaya Matematika i Mekhanika [J. Appl. Math. Mech.]*, 24(6), 1960, 1057-1072 (In Russian).
- [27] Bazhenov, V.G., Balandin, V.V., Grigoryan, S.S., Kotov, V.L. Analiz modeley rascheta dvizheniya tel vrashcheniya minimalnogo soprotivleniya v gruntovykh sredakh [Analysis of models for calculating the motion of solids of revolution of minimum resistance in soil media], *Prikladnaya Matematika i Mekhanika [J. Appl. Math. Mech.]*, 78, 2014, 98-115 (In Russian).
- [28] LS-DYNA Keyword User's Manual, Vol. II, Material Models, LS-DYNA R11 10/12/18 (r:10572), Livermore Software Technology Corporation (LSTC, p.178-182)
- [29] Dyanov, D.Yu., Kotov, V.L. Determination of Nonlinear Strength Characteristics of Sandy Soil Based on the Grigoryan Soil Model, *Problems of Strength and Plasticity*, 82, 2020, 471-482. <https://doi.org/10.32326/1814-9146-2020-82-4-471-482>.

ORCID iD

Aleksandr Konstantinov  <https://orcid.org/0000-0002-3746-2239>



Leonid Igumnov  <https://orcid.org/0000-0003-3035-0119>

Anatoly Bragov  <https://orcid.org/0000-0002-3122-2613>

Victor Eremeyev  <https://orcid.org/0000-0002-8128-3262>

Vladimir Vas. Balandin  <https://orcid.org/0000-0002-3907-3480>

Vladimir Vl. Balandin  <https://orcid.org/0000-0003-3061-8875>



© 2022 Shahid Chamran University of Ahvaz, Ahvaz, Iran. This article is an open access article distributed under the terms and conditions of the Creative Commons Attribution-NonCommercial 4.0 International (CC BY-NC 4.0 license) (<http://creativecommons.org/licenses/by-nc/4.0/>).

How to cite this article: Konstantinov A., Igumnov L., Bragov A., Eremeyev V., Balandin V.V., Balandin V.V. Experimental study and identification of a dynamic deformation model of dry clay at strain rates up to 2500 s⁻¹, *J. Appl. Comput. Mech.*, 8(3), 2022, 981–995. <https://doi.org/10.22055/JACM.2022.39321.3387>

Publisher's Note Shahid Chamran University of Ahvaz remains neutral with regard to jurisdictional claims in published maps and institutional affiliations.

